Brain Research Bulletin 139 (2018) 269–277

Contents lists available at ScienceDirect

Brain Research Bulletin

journal homepage: www.elsevier.com/locate/brainresbull

Research report

Age-dependent changes at the blood-brain barrier. A Comparative structural and functional study in young adult and middle aged rats

Luca Bors[a], Kinga Tóth[b], Estilla Zsófia Tóth[b], Ágnes Bajza[a], Attila Csorba[c], Krisztián Szigeti[d], Domokos Máthé[d,e], Gábor Perlaki[f,g], Gergely Orsi[f,g], Gábor K. Tóth[h], Franciska Erdő[a,*]

[a] Pázmány Péter Catholic University, Faculty of Information Technology and Bionics, Práter u. 50a, H-1083 Budapest
[b] Hungarian Academy of Sciences, Institute of Cognitive Neuroscience and Psychology, Magyar tudósok körútja 2. H-1117 Budapest
[c] University of Szeged, Faculty of Pharmacy, Deparment of Pharmacognosy, Eötvös u. 6, H-6720 Szeged
[d] Semmelweis University, Faculty of Medicine, Department of Biophysics and Radiation Biology, Tűzoltó u. 37-47, H-1094 Budapest,
[e] CROmed Translational Research Ltd. Budapest
[f] MTA-PTE Clinical Neuroscience MR Research Group, Ret u. 2, H-7623 Pecs, Hungary
[g] Department of Neurosurgery, University of Pecs, Medical School, Ret u. 2, H-7623 Pecs, Hungary
[h] Department of Medical Chemistry, Faculty of Medicine, University of Szeged, Dóm tér 8, H-6720, Szeged, Hungary

ARTICLE INFO

Keywords:
Blood-brain barrier
Aging
P-Glycoprotein
Imaging
Microdialysis

ABSTRACT

Decreased beta-amyloid clearance in Alzheimer's disease and increased blood-brain barrier permeability in aged subjects have been reported in several articles. However, morphological and functional characterization of blood-brain barrier and its membrane transporter activity have not been described in physiological aging yet. The aim of our study was to explore the structural changes in the brain microvessels and possible functional alterations of P-glycoprotein at the blood-brain barrier with aging. Our approach included MR imaging for anatomical orientation in middle aged rats, electronmicroscopy and immunohistochemistry to analyse the alterations at cellular level, dual or triple-probe microdialysis and SPECT to test P-glycoprotein functionality in young and middle aged rats. Our results indicate that the thickness of basal lamina increases, the number of tight junctions decreases and the size of astrocyte endfeet extends with advanced age. On the basis of microdialysis and SPECT results the P-gp function is reduced in old rats. With our multiparametric approach a complex regulation can be suggested which includes elements leading to increased permeability of blood-brain barrier by enhanced paracellular and transcellular transport, and factors working against it. To verify the role of P-gp pumps in brain aging further studies are warranted.

1. Introduction

Blood-brain barrier (BBB) dysfunction might be an important component of many neurodegenerative disorders like Alzheimer's disease (Baloyannis, 2015; Miyakawa, 2010; Nelson et al., 2016; Zlokovic, 2011; Erdő et al., 2017), Parkinson's disease (Cabezas et al., 2014; Gray and Woulfe, 2015; Pisani et al., 2012; Erdő et al., 2017), stroke (Lucke-Wold et al., 2014; Enciu et al., 2013; de Jong et al., 1990; Ronaldson and Davis, 2012; Sandoval and Witt, 2008), pharmacoresistant epilepsy (Ates et al., 1999; Michalak et al., 2012; Padou et al., 1995; Sahin et al., 2003; Ndode-Ekane et al., 2010) and multiple sclerosis (Kamphuis et al., 2015; McQuaid et al., 2009; Morgan et al., 2007; Alvarez et al., 2011; Holman et al., 2011). Many of these diseases have an age-related progression (Persidsky et al., 2006). However, in the process of healthy aging there might also be an increased "leakage" of BBB not only by the alteration of endothelial cells, thickness of basal lamina, and morphology of pericytes and astrocytes (Peters et al., 1991), but also due to the changes in expression of different transporter proteins at the endothelial cell layer of BBB. The aim of our study was therefore, to investigate the morphological and functional consequences of advanced age on the blood-brain barrier during the process of physiological aging in healthy rats. This study has a special focus on P-glycoprotein (P-gp,

Abbreviations: ABC, ATP-binding casette; aCSF, artificial cerebrospinal fluid; AP, anterior-posterior; aPPF, artificial peripheral perfusion fluid; AUC, area under the curve; BBB, blood-brain barrier; Cmax, maximum concentration; DMSO, dimethyl sulfoxide; DV, dorso-vetral; FOV, field of view; GFAP, glial fibrillar acidic protein; HESI, heated electrospray ionization; HPLC, high-performance liquid chromatography; IV, intra-venous; LCMS–MS, liquid cromatography–tandem mass spectrometry; LV, lateral ventricle; MDR, multidrug resistance; MIBI, methoxy-isobutyl-isonitrile; ML, midline; MRI, magnetic resonance imaging; NGS, normal goat serum; NHS, normal horse serum; PB, phosphate buffer; P-gp, P-glycoprotein; PRM, parallel reaction monitoring; RF, radiofrequency; SPECT, single photon emission computed tomography; STR, striatum; TJ, tight junctions; TR/TE, repetition time/echo time

* Corresponding author.
E-mail address: erdo.franciska@itk.ppke.hu (F. Erdő).

https://doi.org/10.1016/j.brainresbull.2018.03.001
Received 9 January 2018; Received in revised form 22 February 2018; Accepted 2 March 2018
Available online 06 March 2018

ABCB1/MDR1, Abcb1a/Mdr1a), (the most important efflux transporter) functionality located on the luminal surface of brain capillary endothelial cells. For this approach different techniques were used such as electronmicroscopy and immunohistochemistry for evaluation of morphology and glial fibrillar acidic protein (GFAP) and efflux transporter protein expression; magnetic resonance imaging (MRI) to study macroscopic anatomical alterations of the brain; brain and blood microdialysis to test efflux transporter functions and single photon emission computed tomography (SPECT) imaging also for investigation P-gp efflux transporter functionality at the BBB.

2. Materials and methods

2.1. Comparative MRI in young adult and middle aged rats

MRI was performed on a 3T human MRI scanner (MAGNETOM Trio a Tim System, Siemens AG, Erlangen, Germany) using a loop RF coil with an inner diameter of 40 mm (Siemens Medical Solutions, Erlangen, Germany) and a custom-built head holder (Aradi et al., 2011). T2-weighted images were obtained in three different orientations (i.e. axial, sagittal, coronal) using the following 2D turbo-spin echo sequence: TR/TE = 5270/99 ms; 26 slices; slice thickness = 1 mm; FOV = 34 × 34 mm^2; matrix size = 192 × 192 interpolated to 384 × 384; bandwidth = 40 Hz/pixel; turbo factor = 8; averages = 2.

2.2. Immunohistochemistry

The rats were deeply anesthetized with a high dose of ketamine/xylazine cocktail and transcardially perfused first with physiological saline (3 min), then a fixative containing 4% paraformaldehyde and 15% picric acid in 0.1 M phosphate buffer (PB) (30 min).

60-μm-thick coronal sections were cut from the fixed brain and processed for immunostaining. The P-gp immunostaining was performed according to Volk et al., (2005). In brief, the sections were pretreated with a mixture of 33% acetic acid and 66% ethanol (10 min, −20 °C), followed by the blocking of the endogenous peroxidase enzyme by 0.6% H_2O_2 (30 min) and the blocking of the non-specific immunoglobulin binding of the tissue (60 min) by a mixture of 3% Bovine Serum Albumin (Sigma-Aldrich, St. Louis, MO, USA) and 10% NHS (Normal Horse Serum, Vector Laboratories, Burlingame, CA, USA). The GFAP-immunostaining protocol was performed as described by Grand et al. (2010) with minor modifications (see below). These sections were pre-treated by 1% H_2O_2, followed by a mixture of 2% NGS (Normal Goat Serum, Vector Laboratories, Burlingame, CA, USA) and NHS.

A monoclonal mouse antibody against GFAP (1:2000, EMD Millipore MAB3402, clone GA5, Billerica, MA, USA) or a monoclonal mouse antibody against P-Glycoprotein (P-gp, 1 μg/ml, EMD Millipore MAB517310, clone C219, Billerica, MA, USA) was used as a primary antibody. For the visualization of immunopositive elements, biotinylated anti-mouse immunoglobulin G (1:250, Vector Laboratories) was applied as secondary serum, followed by avidin-biotinylated horseradish peroxidase complex (1:250, Vector Laboratories). The sections were preincubated in 3,30-diaminobenzidine-tetrahydrochloride chromogen (0.05%, Sigma-Aldrich) and then developed by 0.01% H2O2. The P-gp-immunostained sections were mounted, dehydrated for light microscopy (2 × 10 min in xylene) and coverslipped with DePeX (Serva Electrophoresis GmbH, Heidelberg, Germany). The GFAP-immunostained sections were osmicated (0.5%, Electron Microscopy Sciences, Hatfield, PA, USA), dehydrated in ethanol and mounted in Durcupan (Sigma-Aldrich) for further light- and electron microscopic examination. (For more details see: Grand et al., 2010).

2.3. Comparative electronmicroscopy of brain microvasculature of young and middle aged rats

The electron microscopic examination of the blood brain barrier was carried out on two animals (1 young and 1 old adult). The GFAP-stained sections were used. A 400 × 400 μm^2 region was re-embedded from the striatum of both specimens under light microscopic control and sectioned for electron microscopy. Ultrathin serial sections were collected on Formvar-coated single slot grids, stained with lead citrate and examined in a Hitachi 7100 electron microscope. Low- and high magnification (1000×–30,000×) electron micrographs were taken of the capillaries (n = 7 and n = 5 in young- and old animals, respectively).

2.4. Comparative investigation of P-gp function at the BBB in young adult and middle aged rats by in vivo microdialysis

2.4.1. Animals, surgical procedures, and drug administration

Male Wistar rats (ToxiCoop, Budapest, Hungary) 2–3 months (young adult) or 14–16 months (middle aged) were used throughout the experiments and had free access to food and water. CMA/20 peripheral probes were implanted in the jugular vein, and the rats were then placed in a stereotaxic frame for implantation of CMA/12 brain probes in the striatum (STR) or in the lateral ventricle (LV) for performing the microdialysis experiments under chloral hydrate anesthesia (400 mg/kg, intraperitoneal) (Sziráki et al., 2011). The stereotaxic coordinates for STR with respect to the bregma in young rats were AP = +0.20 mm, ML = +3.8, and DV = −7.4. In middle aged rats the position for the STR probe was AP: +0.3 mm, ML: +3.5 mm and DV: −7.5 mm. An additional probe (CMA/12 1 mm membrane) was placed into the LV in the opposite hemisphere to the STR probe in middle aged rats at AP: −1.0 mm, ML: +1.5, DV: −4.0 mm coordinates. Anesthesia during the surgical procedures or the microdialysis experiments was maintained by further injections of chloral hydrate as needed. Quinidine (Sigma-Hungary Kft, Budapest, Hungary, 5 mg/kg), the ABCB1 inhibitor PSC-833 (a gift from Prof. Gábor Tóth, University of Szeged, Hungary, 2 × 2 mg/kg) and vehicle for the inhibitor were administered intravenously (2 mL/kg bodyweight) via a catheter implanted in the femoral vein. All animal experiments were performed in full compliance with the guidelines of the Association for Assessment and Accreditation of Laboratory Animal Care International's expectations for animal use, per the spirit of the licence issued by the Directorate for the Safety of the Food Chain and Animal Health, Budapest and Pest County Agricultural Administrative Authority, Hungary.

2.4.2. Microdialysis procedures and sampling

Animals were sampled from 60 min before till 240 min after intravenous (IV) dosing of quinidine. The peripheral and central probes were perfused with artificial peripheral perfusion fluid (aPPF) or artificial cerebrospinal fluid (aCSF) at a flow rate of 1.0 μL/min using a CMA 102 microdialysis pump. Samples were collected in polyethylene microtubes and placed on dry ice at the end of each collection period. After completing an experiment, the blood and brain dialysates were transferred to a deep freezer and kept at −70 °C. Dialysate samples were later transferred to a bioanalytical laboratory and analyzed for concentrations of quinidine by LCMS–MS.

2.4.3. Data analysis of in vivo experiments

Unpaired Student's *t*-test was performed on areas under the curve (AUCs) of concentration-time profiles, maximum concentrations (Cmax values), individual concentration values and brain-to-blood ratios for testing possible age-dependent differences in concentrations of dialysate samples by the advanced age. The statistical analysis was performed by Microsoft Excel 2010.

At electromicroscopy the following parameters were examined: (i) capillary wall thickness (as a ratio of the inner and outer perimeter of the vessel); (ii) thickness of the basal membrane in spots of 0.5 μm distance from each other along the outer perimeter (281 spots in young and 259 spots in old adults); (iii) area of the astrocyte endfeet profiles (normalized to area of the capillary wall); (iv) area of the pericyte

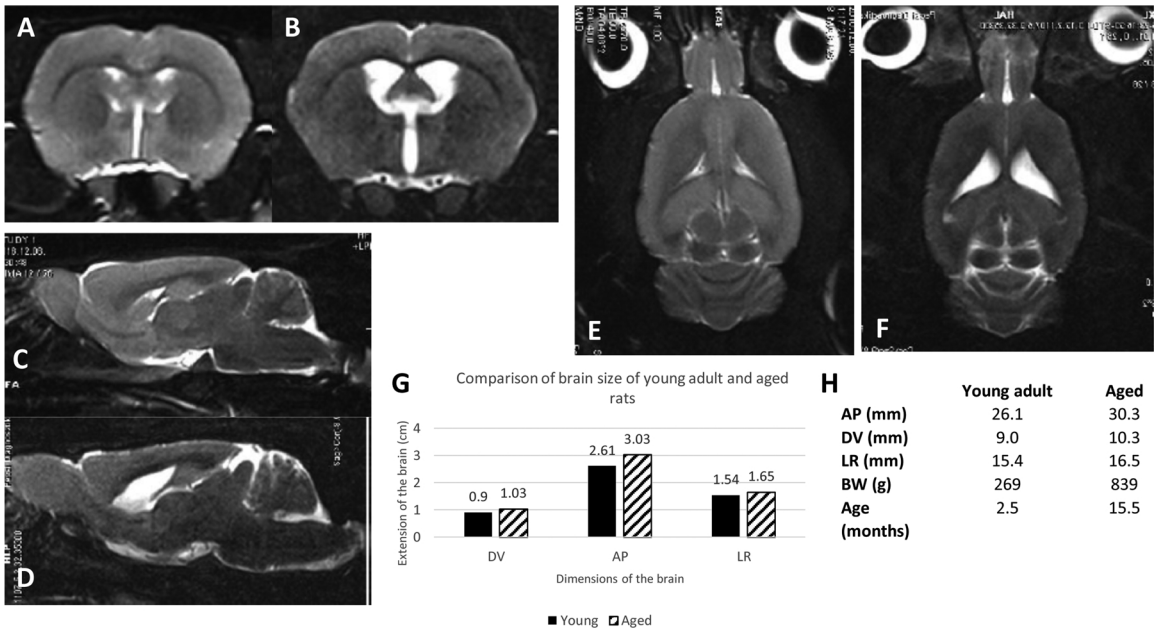

Fig. 1. MR imaging of the brain of a representative young adult and a middle aged Wistar rats. Coronal (A, B), sagittal (C, D) and also axial images (E, F) show a significant difference in the extension of the cerebral ventricles between the young (A, C, E) and middle aged (B, D, F) rats. The difference between the maximum dorso-ventral (DV), anterior-posterior (AP) and lateral (LR) dimensions of the young and old brains are shown in panel G. The comparison of brain size, age and bodyweight of the two observed animals are displayed in panel H.

profiles (normalized to area of the capillary wall); (v) number and length of the TJs (normalized to area of the capillary wall). For the statistical analysis, the nonparametric Mann-Whitney *U* test was applied. Differences were considered to be significant at probability values lower than 0.05.

2.5. LC–MS/MS for bioanalysis of dialysate samples

The quantitative analysis of the dialysate samples was performed on Agilent 1100 HPLC system (Santa Clara, USA) coupled with Thermo Scientific Q Exactive Plus orbitrap mass spectrometer (Waltham, MA USA). The HPLC consisted of binary pump, thermostated autosampler and thermostated column compartment. The column used was Kinetex XB-C18 (particle size 2.6 µm, pore size 100 Å, length/diameter in mm: 50/2.1) from Phenomenex (Gen-Lab Kft., Budapest, Hungary). The isocratic eluent was mixed by the HPLC pump at 0.5 mL/min flow rate in 92/8% A/B ratio where eluent A and B was MS grade water and acetonitrile, respectively, both containing 0.1% formic acid (VWR International Kft., Debrecen, Hungary). The analysis time was 2.5 min. The mass spectrometer operated in positive PRM mode with HESI source (spray voltage: 3500 V, capillary temperature: 300 °C, sheath gas/auxiliary gas/spare gas: 55/15/5 in arbitrary units, sheath gas temperature: 400 °C). The quantitation was done with the *m/z*: 79.0551 Da product ion with 5 ppm mass tolerance from the fragmentation of the *m/z*: 325.1910 Da mass at HCD: 50.

The calibration samples were prepared by spiking aCSF solution in 1% with the working standards. The stock solution had 100 mM concentration in DMSO, the working standards were diluted further in DMSO in 0.025, 0.05, 0.25, 0.5, 2.5, 5, 25, 50, 250, 500 µM concentration. The final concentration range of the calibration samples was 0.25–5000 nM.

2.6. Comparative investigation of P-gp function at the BBB by SPECT imaging in young and middle aged rats

SPECT image acquisition was performed in a NanoSPECT/CT Silver Upgrade system (Mediso, Budapest, Hungary) equipped with rat multi-pinhole apertures. Rats (one young animal as baseline and another young animal dosed with PSC833, one old animal as baseline and another old animal dosed with PSC833) were injected intravenously with [99mTechnetium]-2-methoxy-isobutyl-isonitrile (further referred to as MIBI) with a mean activity of 166.89 MBq. The precursor (Medi-MIBI kit, Medi-Radiopharma Ltd. Érd Hungary) was radiolabeled with ^{99m}Tc-pertechnetate from a ^{99m}Tc-generator (Elumatic III, cisbio international, Gif-sur-Yvette, France) according to the manufacturer's instructions. SPECT skull image acquisitions were started at 12, 24, 36, 48, 60, 72, 84, 96 108 and 120 min post injection. The animal was anaesthetized with 4% isoflurane in medical oxygene while anaesthesia was maintained by 1.8% isoflurane inhalation. The animal was fixed in a Mediso MultiCell (Mediso, Budapest, Hungary) rat bed for exact positioning of the brain in the center of the SPECT field of view. Each SPECT 3D image acquisition took 10 min with 30 raw data acquisition steps. All ten three dimensional images of the skull region were reconstructed using Mediso TeraTomo (Mediso, Budapest, Hungary) SPECT Monte-Carlo simulation based iterative reconstruction algorithm and radioactivity concentrations in MBq/mL were retrieved from the whole brain as region of interest from every SPECT 3D image. Region of interest (ROI) analysis and image processing was performed using the VivoQuant software (inviCRO, Boston, US). Brain ROI radioactivity in function of time and separately at the first two timepoints was then plotted for all scans using OriginPro 8 SR2. AUCs from timepoint 1 (12 min) through to timepoint 10 (120 min) were calculated for all 4 data sets using OriginPro 8 SR2.

3. Results

3.1. MR imaging

The axial, coronal and sagittal images of the brains of a young and a middle aged animals were evaluated. A representative image from all the three orientations are shown in Fig. 1. Comparing the size of the brains, the anterior-posterior extension increased by 14.8%, the lateral extension by 7.1% and the dorso-ventral extension by 14.4% with aging. At the same time the difference between the bodyweights was 3.12 fold. The extension of cerebral ventricles increased significantly with aging which makes the placement of a third microdialysis probe (beside the peripheral and striatal probes) possible exactly into the lateral vetricle in middle aged rats. Due to thickening of the parietal

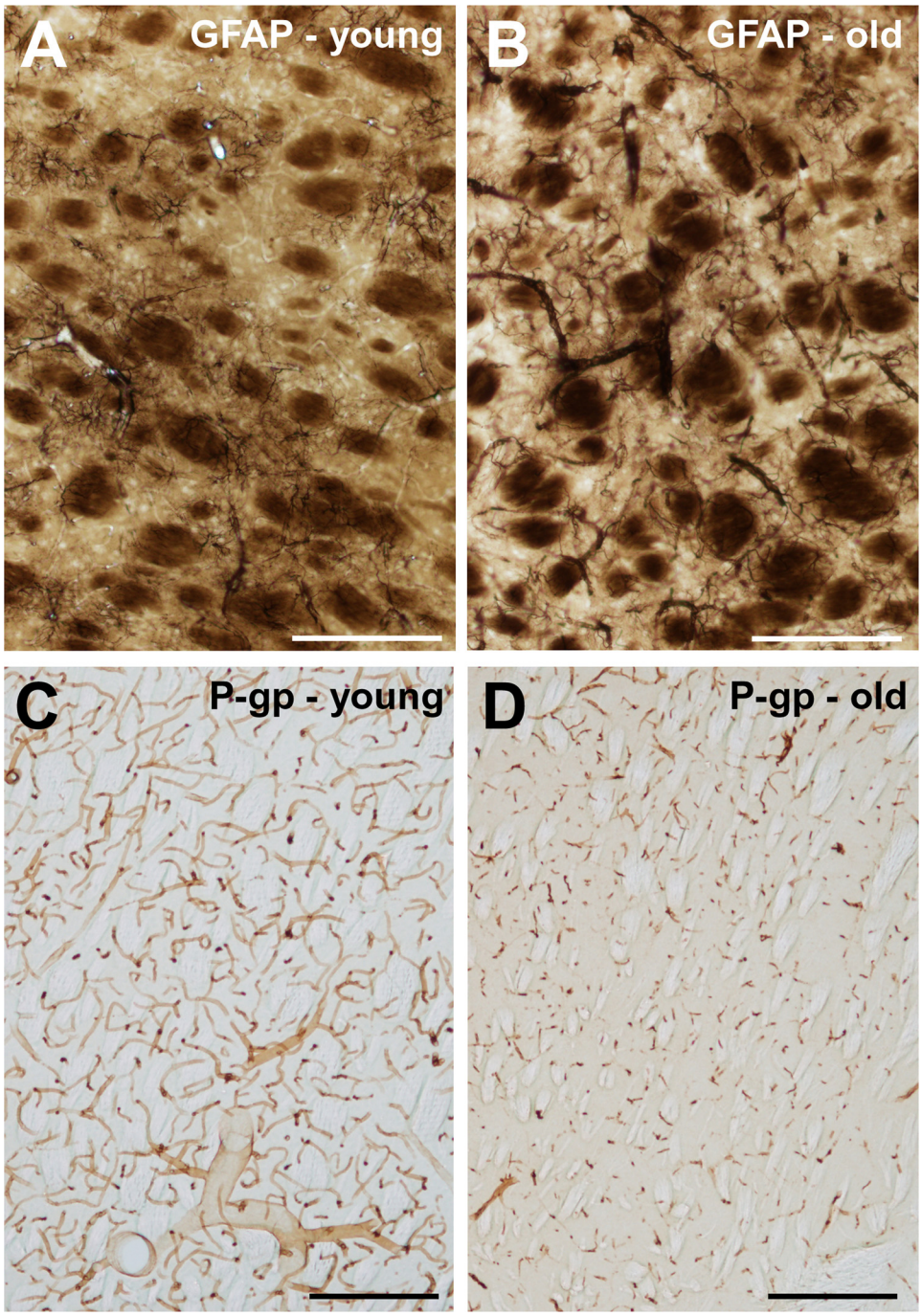

Fig. 2. Light micrographs of the striatum of young adult and middle aged animals, showing astroglial- (A, B) and P-gp-immunostaining (C, D). A: In young adult animals a moderate amount of astroglial elements are found in the striatum. B: In contrast, the astroglial-staining is considerably increased in the brain tissue of old animals. C: An intense staining of the P-gp is visible in the striatum of young adult animals, indicating the high expression level of this efflux transporter protein in the endothelial cells. D: However, a remarkably decreased expression level is found in case of the old animals. Scale: A, B: 200 μm; C, D: 250 μm.

skull bone, the lateral coordiantes of the striatal microdialysis probes was modified in elderly animals from 3.8 to 3.5.

3.2. Light microscopy

P-gp plays an important role in the operation of the BBB by pumping foreign substances out of the endothelial cells (Sarkadi et al., 2006). Astroglial endfeet surrounding the brain capillaries contribute in the functioning of the BBB by providing biochemical support to endothelial cells (Abbott et al., 2006).

Therefore, after the in vivo experiments, we sacrificed the animals and examined and compared the P-gp- and GFAP-staining in the young and middle aged adults.

A moderate amount of astroglial cells and processes were visible in the neocortex (not shown) and in the striatum (Fig. 2A) of the young adult animals. In accordance with the literature (Middeldorp and Hol, 2011), both the amount of astroglial processes and their staining intensity seemed to be increased in the middle aged rats (Fig. 2B).

The P-gp-staining confined to blood vessels in the brain tissues. In case of the young adult animals it was very intense, a high amount of capillaries were immunopositive (Fig. 2C). As it is shown in Fig. 2D, the staining intensity was considerably lower in case of the middle aged

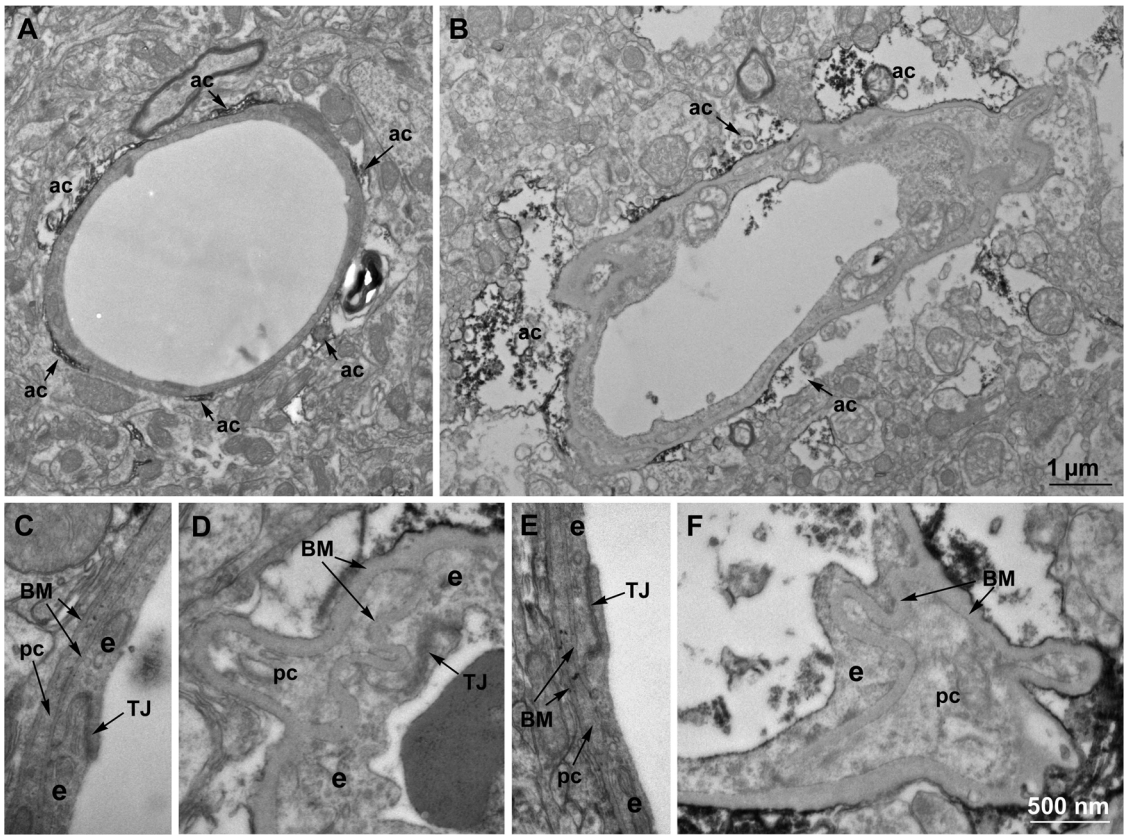

Fig. 3. Low- (A, B) and high magnification (C-F) electron micrographs of brain capillaries of young adult and middle aged animals. A: In case of the young adult animal, the capillary walls are thin and are surrounded by astrocyte endfeet (ac). B: In case of the old animal, the capillary walls are thicker, and the extent of the astrocyte endfeet is considerably higher. C, E: A segment of the capillary wall in young adult animal at a 30.000-fold magnification. A tight junction (TJ) is visible sealing the adjacent endothelial cells (e). On the opposite side of the lumen, a pericyte (pc) can be observed embedded in the basal membrane (BM). D, F: A segment of the capillary wall in old animal at a 30.000-fold magnification. Smaller amount of tight junctions are visible among the endothelial cells. The basal membrane is considerably thicker compared to young adult animal and like in the young specimens often surround pericytes. Scale: A, B: 1 µm; C-F: 500 nm.

animals, suggesting a lower expression of this efflux transporter protein by the increasing age (Silverberg et al., 2010).

3.3. Electronmicroscopy

The ultrastructural composition of the blood brain barrier was altered in the old animal (Fig. 3).

The wall of the microvessels are composed of the regular elements, such as the endothelial cells connected by tight junctions (TJ), pericytes embedded in the basal membrane and the basal membrane which bounds the capillary from the side of the brain parenchima. The capillaries were surrounded by GFAP-immunopositive astroglial endfeet.

The thickness of the capillary walls was calculated as a ratio of the inner and outer perimeter of the vessel to avoid getting false results due to measuring vessels of different size. Values nearing 1 depict a thin wall, whereas lower values depict a thicker wall. We found that the thickness of the capillary walls was significantly increased in the old animal (0.88 ± 0.05 vs 0.57 ± 0.14 in young and middle aged adults, respectively, $p = 0.0058$) (Fig. 3A, B).

The thickness of the basal membrane also increased significantly in case of the old animal (24.3 ± 8.8 nm vs 93.9 ± 34.1 nm in young and middle aged adults, respectively, $p = 0.0001$) (Fig. 3C–F).

In the old animal, the area of the astrocyte endfeet profiles surrounding the capillaries was significantly higher, than in the young animal (3.54 ± 3.42 μm^2 vs 0.47 ± 1.06 μm^2; $p = 0.0001$). The difference was statistically significant even after normalizing to the area of the capillary wall (1.58 ± 1.14 vs 0.48 ± 0.65; $p = 0.0348$) (Fig. 3A, B).

The amount of pericytes did not show any changes. The absolute values of perycite profile areas did not change (0.36 ± 0.41 μm^2 in young- and 0.54 ± 0.44 μm^2 in old animal; $p = 0.1012$). Similarly the values normalized to the area of the capillary wall (0.15 ± 0.04 vs 0.17 ± 0.07 in young and middle aged adults, respectively, $p = 0.5698$) did not significantly change.

Finally, we examined the tight junctions and found a decreased amount between the endothelial cells in case of capillaries of the old animal. The average length of the TJs did not show a difference in the young and old animal (0.44 ± 0.35 µm vs 0.41 ± 0.51 µm; $p = 0.4038$). However, both the number of TJs (0.35 ± 0.29 vs 0.1 ± 0.2; $p = 0.0740$) and their total length per capillary (0.11 ± 0.04 vs 0.04 ± 0.06; $p = 0.0740$) displayed a decreasing tendency in the old animal (values are normalized to area of the capillary wall), although the differences were not significant.

In summary, the ultrastructural composition of the blood brain barrier changed in the old animal. The capillary walls and the basal membranes were thicker, the size of astrocyte endfeet around the vessels extended and the connection of endothelial cells by tight junctions displayed a decreasing tendency.

3.4. LC–MS/MS results

For determination of quinidine concentration in dialysate samples an LC–MS/MS method was developed. The calibration was accepted with R^2 value higher than 0.995. The calibration model was non-linear due to the wide concentration range. The typical chromatograms are shown in Fig. 4.

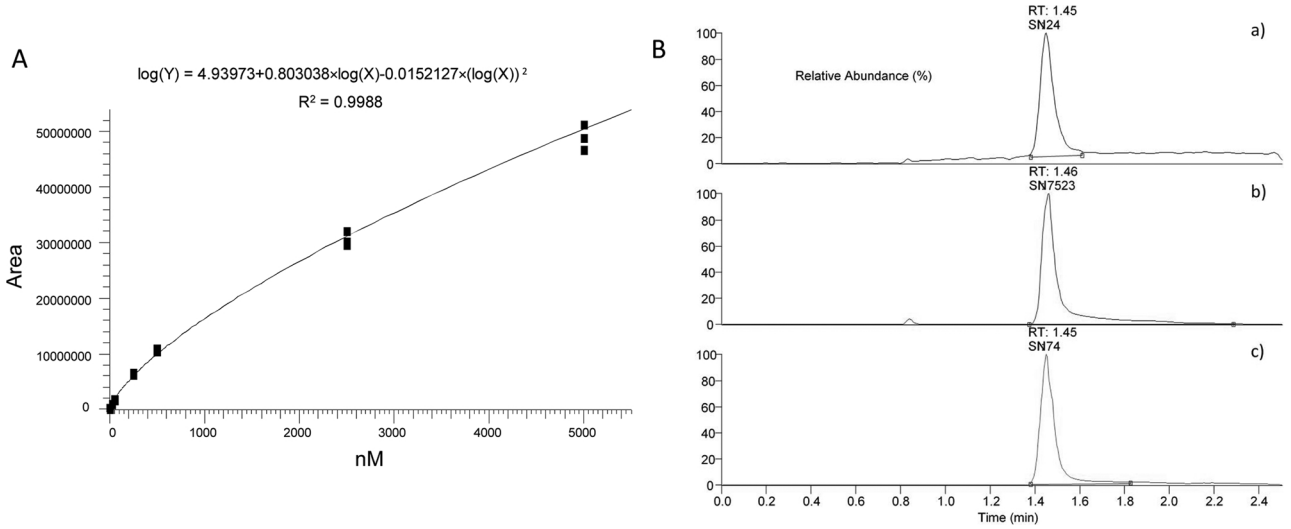

Fig. 4. LCMS-MS analysis of microdialysis samples. Calibration curve used for quantitation of dialysate samples (panel A). Typical chromatograms of the a) lowest calibration level (0.25 nM), b) highest calibration level (5000 nM) and c) dialysate sample (panel B).

3.5. Microdialysis

The concentration-time profiles of quinidine in the striatum, in the plasma and the lateral ventricle are shown in Fig. 5. The AUC_{STR}/AUC_{blood} ratio in control rats was 24.2% (young) and 29.6% (old), respectively. The brain exposure was higher in middle aged animals than in young ones in control groups (AUC_{STR} = 124.82 vs 75.12 nM h), but not in the PSC-833 treated groups (420.61 vs 530.96 nM h). In the groups of P-gp inhibitor treated animals the AUC_{STR}/AUC_{blood} ratio was enhanced to 76.0% (young) and 91.0% (old), respectively. The striatal concentrations of quinidine increased in a statistically significant manner both in young ($p < 0.05$) and in middle aged ($p < 0.005$) rats after the administration of the inhibitor as it is seen from the AUC_{STR} values (Fig. 5). Also the elimination of the drug from the brain and blood shows a slower kinetics in the case of P-gp inhibition. The difference between the striatal concentration values of old and young controls was statically significant ($p < 0.05$) at later timepoints (120 and 150 min after QND treatment) (Fig. 5A,C) reflecting to a higher, and longer lasting exposure to P-gp substrate with advanced age. The blood levels seemed also to be higher in aged than in the young

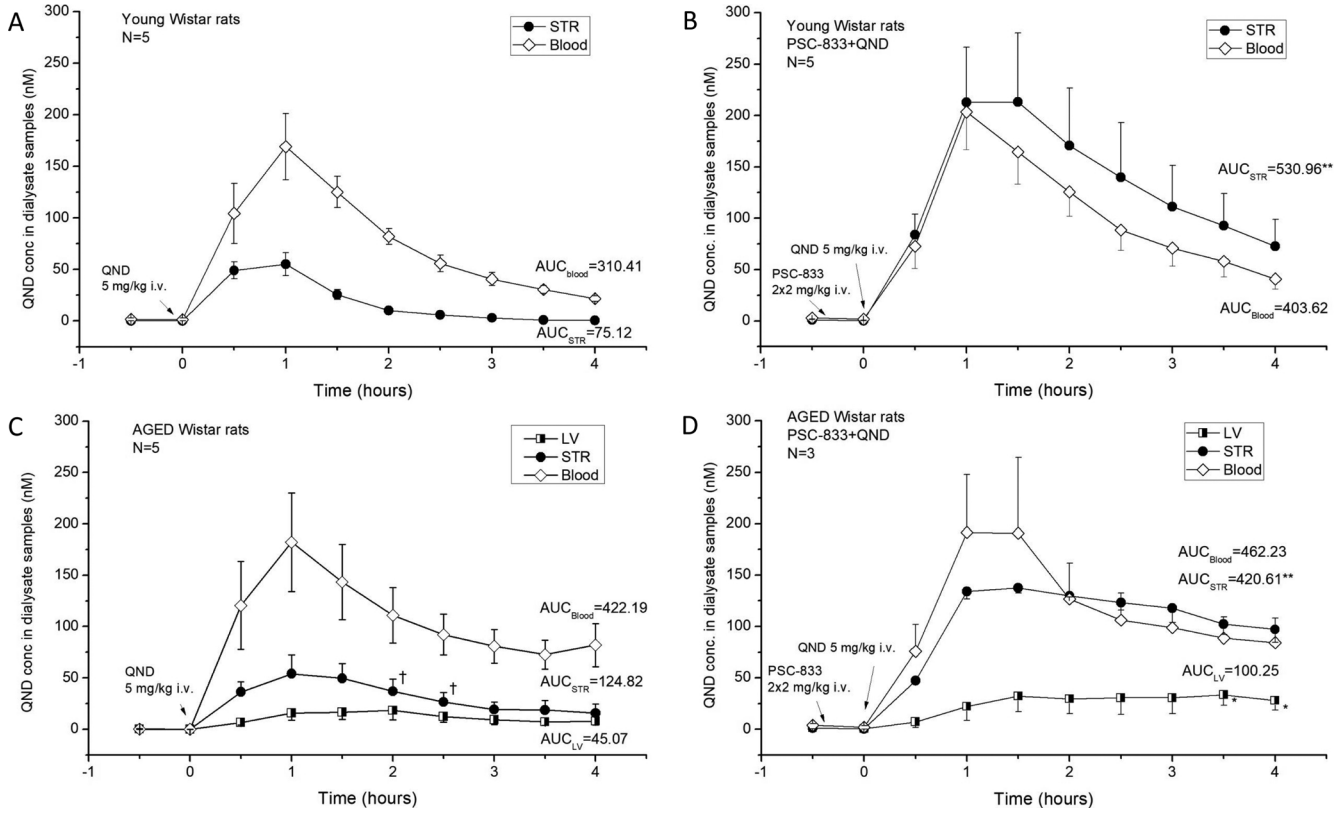

Fig. 5. Concentration-time profiles of quinidine (QND) (5 mg/kg i.v.) in young (A, B) and middle aged (C, D) Wistar rats in absence (A,C) and presence (B,D) of PSC-833 (2x2 mg/kg i.v).The values are mean concentrations +/- SEM, N = 3–5/group. *: $p < 0.05$, **:$p < 0.005$ by T-test (control group compared to PSC-833 treated group), $p < 0.05$ young controls v.s. middle aged controls. STR: striatum, LV: lateral ventricle, AUC: area under the curve, QND: quinidine.

subjects, but the difference was not statistically significant.

The different orientation of P-gp pump in the choroid plexus (blood − cerebrospinal fluid barrier, BSCFB) and in the BBB has been reported. (Shen et al., 2009; Krajcsi et al., 2012) At the BCSFB the pumping function of P-gp is oriented from the blood to the liquor, in contrast at the BBB endothelial cells P-gp mediates the transport of its substrates into the opposite direction, towards the blood. Therefore, we compared the AUC ratio of quinidine for CSF (in the lateral ventricle) to blood and for brain parenchyma (STR) to blood in presence and absence of PSC-833 in the middle aged animals. The AUC_{LV}/AUC_{blood} showed a 2.03 fold increase and the AUC_{STR}/AUC_{blood} displayed a 3.08 fold increase after PSC-833 treatment (Fig. 5C,D). These data suggest that although the orientation is different there are other mechanisms too, playing a role in quinidine disposition in the CNS.

In summary, our results indicate a moderate difference in the BBB permeability between the young and old subjects for our P-gp substrate, quinidine in control animals. However, if the transporter is chemically blocked by a specific inhibitor the increase of brain exposure becomes higher in young than in elderly subjects. These findings are in accordance with the lower expression level of P-gp in elderly animals (our unpublished data) and reduced P-gp function reported in aged humans (Toornvliet et al., 2006; Bartels et al., 2009). The blockade of lower number of efflux transporter proteins results in a lower increase in the BBB permeation for quinidine in old rats compared to the young adults.

3.6. SPECT imaging

The brain exposure to MIBI in presence and absence of P-gp inhibitor was evaluated in one-one representative animal by SPECT imaging. The radioactivity in the brain increased both in young and in old rats after administration of P-gp −inhibitor as it is seen in the MIBI efflux curves (Fig. 6). At the first timepoint the control exposure is higher in young rats suggesting a slower kinetics, but after 24–36 min the MIBI level becomes higher in the brain of the middle aged animal indicating a higher leakage of the BBB in the old subject. The order of P-gp functionality in young and old animals is the following: young control > old control > old PSC–833 = young PSC-833 as it is seen in Fig. 6. These results indicate a higher transcellular permeability of the BBB endothelial cells for P-gp substrates in advanced age and a reduced P-gp expression or function with aging leading to similar brain exposure of MIBI to young subjects after chemical blocking of the transporter.

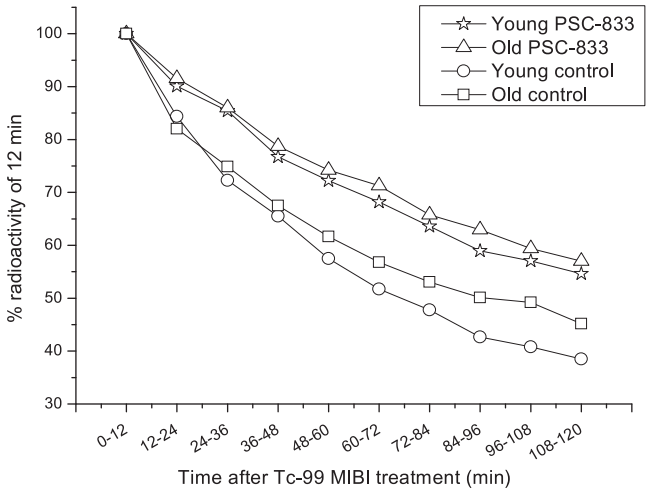

Fig. 6. Brain exposure to [99 mTechnetium]-2-methoxy-isobutyl-isonitrile (MIBI) as measured by radioactivity of the brain in 0-120 min after intravenous administartion of the tracer in young and middle aged animals treated or non-treated with PSC-833. Brain radioactivity is expressed as a percent of the radioactivity detected in the brain in the first measuring period (0-12 min).

4. Discussion

Our study described here, focused on the investigation ofalteration of the different cerebrovascular parameters and factors with physiological aging. Our model animals were male Wistar rats. They were housed in pairs in their home cages. The keeping was at least 14–16 months long at our animal facility and during this period the animals have ad libitum access to standard laboratory food and tap water. According to the observations of Sengupta (2013), the age of the rats can be correlated with the age of humans. In that study a comparison between *Rattus Norvegicus* and humans was made. The study also observed age-dependent correlations between the days of rat age and the years of human age. Different other methods of calculation for comparing the human and rat age have also been published. However, we have not been able to identify any study on the comparison of different rat strains, although it is well known that the bodyweight and body size development are very variable between different rat strains. On the basis of data available (Sengupta, 2013) we conclude that our experimental rats were middle aged (approximately 50- year old in humans).

Our results confirmed the data of the literature concerning the effect of aging on ultrastuctural changes in the brain microvasculature (Hunziker et al., 1978; Kacem et al., 1998) and the GFAP and P-gp expression in the BBB (Peinado et al., 1998; Tigges et al., 1995). On the basis of these results our middle aged male Wistar rats seems to be appropriate model animals of healthy, physiological aging. To charachterize the P-gp function relative to aging a previously validated probe substrate, quinidine (ki et al., 2011, 2013;) was used in microdialysis experiments and [^{99m}Technetium]-2-methoxy-isobutyl-isonitrile (Tc-MIBI) (Piwnica-Worms and Sharma, 2010) was applied as a SPECT radiotracer. Both compounds displayed a low brain exposure in control animals and an enhanced brain level after P-gp inhibition. A slower distribution of MIBI can be seen in aged animals then in young ones in the first some minutes after treatment (probably due to the decreased blood flow in aged rat), but 24 min after the intravenous injection a higher brain penetration was reached in the middle aged rat. The brain exposure to MIBI is influenced by several factors like (i) regional blood flow (ii) cellular mitochondrial number per unit organ mass (ii) cellular membrane potential (iii) mitochondrial membrane potential (iv) cell membrane lipid bilayer fluidity (v) cellular Na/H antiporter activity and (vi) P-gp efflux pump expression and function (Piwnica-Worms et al., 1990; Kurata et al., 2015). It has been described that the cerebral blood flow value is smaller in old subjects (Jefferson et al., 2017) than is young ones, therefore and due to an increased thickness of the basal lamina and capillary walls (including cell membrane thickness increase) and the astrocyte endfeet, MIBI inflow slowers in old animals. In microdialysis study, the control level of quinidine is higher in old than in young adult rats as it is seen from the AUC values (Fig. 5A, C). However, these values are generated from a 240 min period of time of concentration-time profiles which includes the absorption, distribution and also the elimination phases of quinidine both in the brain parenchyma (STR) and in the cerebrospinal fluid (LV). The concentration differences are higher at the later timepoints indicating a slower elimination in old rats.

Immunostainings, ultrastructural, microdialysis and SPECT results taken together suggest that there are many remarkable differences in the structure and function of the blood-brain barrier in young and old rats. These differences can be detected at the level of endothelial cells, astrocytes, tight junctions, basal membrane and efflux transporters. Several structural and morphological alterations lead to a stronger protection of the brain with aging, while other domains like P-gp downregulation and lower expression of tight junction proteins result in higher BBB permeability in aged subjects. The paracellular permeability of BBB seems to be higher and the transcellular transport is increased due to the reduced P-gp function with aging which can be a starting point of the influx of xenobiotics and different dangerous endogenous and exogenous compounds to the brain. To decide whether the

increasing BBB leakage initiate or enforce the serious events of age-related neurodegenerative processes further studies are needed in animals with at an even more advanced age. Studies focusing on the analysis of the changes in cognitive function and behavioral performance of middle aged Wistar rats are warranted. Environmental factors playing an important role in the effect of aging on our mental health should also be considered.These factors, such as the effect of physical activity, caloric restriction or cadmium intake of smokers should also be taken into account and studied in details in the future.

Our present study has shed light on age-related differences in the BBB and also pointed out the complexity of the topic.

Author contribution statement

LB (microdialysis, statistical analysis, figures) 20%, KT (electronmicroscopy) 8%, EZsT (immunohistochemistry) 5%, ÁB (microdialysis) 7%, ACs (bioanalysis) 10%, KSz (SPECT) 5%, DM (SPECT) 5%, GP (MRI) 5%, GO (MRI) 5%, GKT (PSC-833 synthesis) 5% and FE (microdialysis, writing, figures) 25%.

Declaration of interest

None.

Acknowledgements

The authors thank the Faculty of Information Technology and Bionics, Pázmány Péter Catholic University, Budapest, Hungary for the support of the publication costs of this article.

This work was supported by the European Union through grant no. EFOP-3.6.3-VEKOP-16-2017-00002 co-financed by the European Social Fund.

This paper was also supported by the ÚNKP- 17-4-I-PTE-76 and ÚNKP-17-4-III-PTE-93 New National Excellence Program of the Ministry of Human Capacities, the János Bolyai Research Scholarship of the Hungarian Academy of Sciences (G.P. and G.O.), PTE ÁOK-KA-2017-05 and PTE ÁOK-KA-2017-06. Mediso Ltd., Budapest, Hungary is also acknowledged for the high level provision and maintenance of the SPECT/CT system.

References

Abbott, N.J., Rönnbäck, L., Hansson, E., 2006. Astrocyte-endothelial interactions at the blood-brain barrier. Nat. Rev. Neurosci. 7 (1), 41–53.

Alvarez, J.I., Cayrol, R., Prat, A., 2011. Disruption of central nervous system barriers in multiple sclerosis. Biochim. Biophys. Acta 1812 (2), 252–264.

Aradi, M., Steier, R., Bukovics, P., Szalay, C., Perlaki, G., Orsi, G., Pal, J., Janszky, J., Doczi, T., Schwarcz, A., 2011. Quantitative proton MRI and MRS of the rat brain with a 3T clinical MR scanner. J. Neuroradiol. 38, 90–97.

Ates, N., Esen, N., Ilbay, G., 1999. Absence epilepsy and regional blood-brain barrier permeability: the effects of pentylenetetrazole-induced convulsions. Pharmacol. Res. 39 (4), 305–310.

Baloyannis, S.J., 2015. Brain capillaries in Alzheimer's disease. Hell. J. Nucl. Med. 18, 152.

Bartels, A.L., Kortekaas, R., Bart, J., Willemsen, A.T., de Klerk, O.L., de Vries, J.J., van Oostrom, J.C., Leenders, K.L., 2009. Blood-brain barrier P-glycoprotein function decreases in specific brain regions with aging: a possible role in progressive neurodegeneration. Neurobiol. Aging 30 (11), 1818–1824.

Cabezas, R., Avila, M., Gonzalez, J., El-Bacha, R.S., Baez, E., Garcia-Segura, L.M., Jurado Coronel, J.C., Capani, F., Cardona-Gomez, G.P., Barreto, G.E., 2014. Astrocytic modulation of blood brain barrier: perspectives on Parkinson's disease. Front. Cell. Neurosci. 8, 211.

de Jong, G.I., Horvath, E., Luiten, P.G., 1990. Effects of early onset of nimodipine treatment on microvascular integrity in the aging rat brain. Stroke 21 (Suppl. 12), 113–116 (pp. IV).

Enciu, A.M., Gherghiceanu, M., Popescu, B.O., 2013. Triggers and effectors of oxidative stress at blood-brain barrier level: relevance for brain ageing and neurodegeneration. Oxid. Med. Cell. Longev. p297512.

Erdő, F., Denes, L., de Lange, E., 2017. Age-associated physiological and pathological changes at the blood-brain barrier: a review. J. Cereb. Blood Flow Metab. 37 (1), 4–24.

Grand, L., Wittner, L., Herwik, S., Göthelid, E., Ruther, P., Oscarsson, S., Neves, H., Dombovári, B., Csercsa, R., Karmos, G., Ulbert, I., 2010. Short and long term biocompatibility of NeuroProbes silicon probes. J. Neurosci. Methods 189 (2), 216–229.

Gray, M.T., Woulfe, J.M., 2015. Striatal blood-brain barrier permeability in Parkinson's disease. J. Cereb. Blood Flow Metab. 35 (5), 747–750.

Holman, D.W., Klein, R.S., Ransohoff, R.M., 2011. The blood-brain barrier, chemokines and multiple sclerosis. Biochim. Biophys. Acta 1812 (2), 220–230.

Hunziker, O., Abdel'Al, S., Frey, H., Veteau, M.J., Meier-Ruge, W., 1978. Quantitative studies in the cerebral cortex of aging humans. Gerontology 24 (1), 27–31.

Jefferson, A.L., Liu, D., Gupta, D.K., Pechman, K.R., Watchmaker, J.M., Gordon, E.A., Rane, S., Bell, S.P., Mendes, L.A., Davis, L.T., Gifford, K.A., Hohman, T.J., Wang, T.J., Donahue, M.J., 2017. Lower cardiac index levels relate to lower cerebral blood flow in older adults. Neurology 89 (23), 2327–2334.

Kacem, K., Lacombe, P., Seylaz, J., Bonvento, G., 1998. Structural organization of the perivascular astrocyte endfeet and their relationship with the endothelial glucose transporter: a confocal microscopy study. Glia 23 (1), 1–10.

Kamphuis, W.W., Derada Troletti, C., Reijerkerk, A., Romero, I.A., de Vries, H.E., 2015. The blood-brain barrier in multiple sclerosis: microRNAs as key regulators. CNS Neurol. Disord. Drug Targets 14 (2), 157–167.

Krajcsi, P., Jani, M., Tóth, B., Erdő, F.K.E., Beéry, E., Sziráki, I., 2012. óEfflux transporters in the blood-brain interfaces–in vitro and in vivo methods and correlations. Expert Opin. Drug Metab. Toxicol. 8 (4), 419–431.

Kurata, S., Ushijima, K., Kawahara, A., Kaida, H., Kawano, K., Hirose, Y., Kage, M., Kamura, T., Ishibashi, M., Abe, T., 2015. Assessment of 99mTc-MIBI SPECT(/CT) to monitor multidrug resistance-related proteins and apoptosis-related proteins in patients with ovarian cancer: a preliminary study. Ann. Nucl. Med. 29 (7), 643–649.

Lucke-Wold, B.P., Logsdon, A.F., Turner, R.C., Rosen, C.L., Huber, J.D., 2014. Aging, the metabolic syndrome, and ischemic stroke: redefining the approach for studying the blood-brain barrier in a complex neurological disease. Adv. Pharmacol. 71, 411–449.

McQuaid, S., Cunnea, P., McMahon, J., Fitzgerald, U., 2009. The effects of blood-brain barrier disruption on glial cell function in multiple sclerosis. Biochem. Soc. Trans. 37 (1), 329–331.

Michalak, Z., Lebrun, A., Di Miceli, M., Rousset, M.C., Crespel, A., Coubes, P., Henshall, D.C., Lerner-Natoli, M., Rigau, V., 2012. IgG leakage may contribute to neuronal dysfunction in drug-refractory epilepsies with blood-brain barrier disruption. J. Neuropathol. Exp. Neurol. 71 (9), 826–838.

Middeldorp, J., Hol, E.M., 2011. GFAP in health and disease. Prog. Neurobiol. 93 (3), 421–443.

Miyakawa, T., 2010. Vascular pathology in Alzheimer's disease. Psychogeriatrics 10 (1), 39–44.

Morgan, L., Shah, B., Rivers, L.E., Barden, L., Groom, A.J., Chung, R., Higazi, D., Desmond, H., Smith, T., Staddon, J.M., 2007. Inflammation and dephosphorylation of the tight junction protein occludin in an experimental model of multiple sclerosis. Neuroscience 147 (3), 664–673.

Ndode-Ekane, X.E., Hayward, N., Grohn, O., Pitkanen, A., 2010. Vascular changes in epilepsy: functional consequences and association with network plasticity in pilocarpine-induced experimental epilepsy. Neuroscience 166 (1), 312–332.

Nelson, A.R., Sweeney, M.D., Sagare, A.P., Zlokovic, B.V., 2016. Neurovascular dysfunction and neurodegeneration in dementia and Alzheimer's disease. Biochim. Biophys. Acta 1862 (5), 887–900.

Padou, V., Boyet, S., Nehlig, A., 1995. Changes in transport of [14C] alpha-aminoisobutyric acid across the blood-brain barrier during pentylenetetrazol-induced status epilepticus in the immature rat. Epilepsy Res. 22 (3), 175–183.

Peinado, M.A., Quesada, A., Pedrosa, J.A., Torres, M.I., Martinez, M., Esteban, F.J., Del Moral, M.L., Hernandez, R., Rodrigo, J., Peinado, J.M., 1998. Quantitative and ultrastructural changes in glia and pericytes in the parietal cortex of the aging rat. Microsc. Res. Tech. 43 (1), 34–42.

Persidsky, Y., Ramirez, S.H., Haorah, J., Kanmogne, G.D., 2006. Blood-brain barrier: structural components and function under physiologic and pathologic conditions. J. Neuroimmune Pharmacol. 14 (2), 223–267.

Peters, A., Josephson, K., Vincent, S.L., 1991. Effects of aging on the neuroglial cells and pericytes within area 17 of the rhesus monkey cerebral cortex. Anat. Rec. 229 (3), 384–398.

Pisani, V., Stefani, A., Pierantozzi, M., Natoli, S., Stanzione, P., Franciotta, D., 2012. Increased bloodcerebrospinal cerebrospinal fluid transfer of albumin in advanced Parkinson's disease. J. Neuroinflamm. 9, 188.

Piwnica-Worms, D., Sharma, V., 2010. Probing multidrug resistance P-glycoprotein transporter activity with SPECT radiopharmaceuticals. Curr. Top. Med. Chem. 10 (17), 1834–1845.

Piwnica-Worms, D., Kronauge, J.F., Delmon, L., Holman, B.L., Marsh, J.D., Jones, A.G., 1990. Effect of metabolic inhibition on technetium-99m-MIBI kinetics in cultured chick myocardial cells. J. Nucl. Med. 31 (4), 464–472.

Ronaldson, P.T., Davis, T.P., 2012. Blood-brain barrier integrity and glial support: mechanisms that can be targeted for novel therapeutic approaches in stroke. Curr. Pharm. Des. 18 (25), 3624–3644.

Sahin, D., Sahin, D., Ilbay, G., Ates, N., 2003. Changes in the blood-brain barrier permeability and in the brain tissue trace element concentrations after single and repeated pentylenetetrazole-induced seizures in rats. Pharmacol. Res. 48 (1), 69–73.

Sandoval, K.E., Witt, K.A., 2008. Blood-brain barrier tight junction permeability and ischemic stroke. Neurobiol. Dis. 32 (2), 200–219.

Sarkadi, B., Homolya, L., Szakács, G., Váradi, A., 2006. Human multidrug resistance ABCB and ABCG transporters: participation in a chemoimmunity defense system. Physiol. Rev. 86 (4), 1179–1236.

Sengupta, P., 2013. The laboratory rat: relating its age with human's. Int. J. Prev. Med. 4 (6), 624–630.

Shen, J., Carcaboso, A.M., Hubbard, K.E., Tagen, M., Wynn, H.G., Panetta, J.C., Waters, C.M., Elmeliegy, M.A., Stewart, C.F., 2009. Compartment-specific roles of ATP-

binding cassette transporters define differential topotecan distribution in brain parenchyma and cerebrospinal fluid. Cancer Res. 69 (14), 5885–5892.
Silverberg, G.D., Miller, M.C., Messier, A.A., Majmudar, S., Machan, J.T., Donahue, J.E., Stopa, E.G., Johanson, C.E., 2010. Amyloid deposition and influx transporter expression at the blood-brain barrier increase in normal aging. J. Neuropathol. Exp. Neurol. 69 (1), 98–108.
Sziráki, I., Erdő, F., Beéry, E., Molnár, P.M., Fazekas, C., Wilhelm, I., Makai, I., Kis, E., Herédi-Szabó, K., Abonyi, T., Krizbai, I., Tóth, G.K., Krajcsi, P., 2011. Quinidine as an ABCB1 probe for testing drug interactions at the blood-brain barrier: an in vitro in vivo correlation study. J. Biomol. Screen. 16 (8), 886–894.
Sziráki, I., Erdő, F., Trampus, P., Sike, M., Molnár, P.M., Rajnai, Z., Molnár, J., Wilhelm, I., Fazakas, C., Kis, E., Krizbai, I., Krajcsi, P., 2013. The use of microdialysis techniques in mice to study P-gp function at the blood-brain barrier. J. Biomol. Screen. 18 (4), 430–440.
Tigges, J., Herndon, J.G., Rosene, D.L., 1995. Mild age-related changes in the dentate gyrus of adult rhesus monkeys. Acta Anat. (Basel) 153 (1), 39–48.
Toornvliet, R., van Berckel, B.N., Luurtsema, G., Lubberink, M., Geldof, A.A., Bosch, T.M., Oerlemans, R., Lammertsma, A.A., Franssen, E.J., 2006. Effect of age on functional P-glycoprotein in the blood-brain barrier measured by use of (R)-[(11)C]verapamil and positron emission tomography. Clin. Pharmacol. Ther. 79 (6), 540–548.
Volk, H., Potschka, H., Löscher, W., 2005. Immunohistochemical localization of P-glycoprotein in rat brain and detection of its increased expression by seizures are sensitive to fixation and staining variables. J. Histochem. Cytochem. 53 (4), 517–531.
Zlokovic, B.V., 2011. Neurovascular pathways to neurodegeneration in Alzheimer's disease and other disorders. Nat. Rev. Neurosci. 12 (12), 723–738.